Advanced Composites and Hybrid Materials (2020) 3:8–15
https://doi.org/10.1007/s42114-020-00141-9

ORIGINAL RESEARCH

Characterization and antibacterial activity of rice grain-shaped ZnS nanoparticles immobilized inside the polymer electrospun nanofibers

Gopal Panthi[1] · Rosa Ranjit[2] · Subash Khadka[2] · Kapil Raj Gyawali[3] · Hak-Yong Kim[4] · Mira Park[1]

Received: 21 February 2019 / Revised: 9 January 2020 / Accepted: 20 January 2020 / Published online: 27 January 2020

Abstract

Present work introduces the fabrication of antibacterial nanofibers composite of poly(vinyl acetate) doped with in situ-synthesized rice grain-shaped ZnS nanoparticles using electrospinning technique. FE-SEM and TEM analyses revealed that the ZnS nanoparticles were uniformly incorporated inside the polymer nanofibers. The antibacterial activity of as-fabricated nanofibers composite was investigated under indoor light activation towards Gram-negative (*E. coli*) and Gram-positive (*S. aureus*) bacteria. Such strategy for immobilizing ceramic nanoparticles inside polymer nanofibers might be helpful to overcome the photocorrosion and recovery problems of ZnS-based materials.

Keywords Electrospinning · ZnS · Antibacterial · Semiconductor · Chemical synthesis

1 Introduction

Nanomaterials have been extensively used in medicine, sensors, electronic devices, and energy storage devices because of their distinctive physical and chemical properties compared to their bulk materials. Therefore, various nanomaterials are designed to find their applications in many commercial products, such as electronics, drug delivery, cosmetics, protective clothing, and sporting goods [1, 2]. In this regard, numerous studies have been done on the nanostructured semiconductors, and many papers have been published on nanostructured ZnO and TiO_2 semiconductors in the recent literature because of their useful properties and technological importance [3–6]. Among these, II-IV semiconductors nanoparticles especially ZnS and ZnO are well-considered as nontoxic, bio-safe, and biocompatible to be used in biological fields [7–9]. For instance, the first discovered and widely studied semiconductor material ZnS with a band gap of 3.8 eV has emerged as a potential antibacterial material due to its deeper conduction and valence bands as compared to other semiconductors including ZnO and TiO_2 [10–13]. Also, ZnS is of major interest in biomedical, electronics, and photovoltaic devices due to its luminescent and catalytic properties [14–16].

The phenomena of aggregation and photocorrosion are likely to occur in nanostructural materials, which lead to minimize their performance. Therefore, various efforts have been made to overcome these difficulties by combining ZnS nanoparticles with other semiconductors [17], incorporating in mesoporous materials [18, 19] or polymer matrix [20], forming composites with graphene [21] or CNT [22] and applying alternative preparation techniques [23, 24]. Studies have revealed that polymers, when applied as templates, can confine the nanoparticles precipitated in them. In addition, some polymers can maintain a certain superstructure and produce inorganic-polymer hybrids showing interesting morphologies [25, 26]. Regarding this, various reports have been published for synthesizing semiconductor-polymer nanocomposites and their applications in electronics, optics, and catalysts. Besides, electrospinning is a convenient method to fabricate polymer nanofibers encapsulated with nanostructured materials [27, 28].

✉ Mira Park
wonderfulmira@jbnu.ac.kr

[1] Department of Biomedical Sciences and Institute for Medical Science, Chonbuk National University, Jeonju 54907, South Korea

[2] Natural Product Research Laboratory, Faculty of Science, Nepal Academy of Science and Technology (NAST), Khumaltar, GPO Box 3323, Lalitpur, Nepal

[3] Department of Chemistry, Birendra Multiple Campus, Tribhuvan University, Bharatpur, Chitwan, Nepal

[4] Department of Organic Materials and Fiber Engineering, Chonbuk National University, Jeonju 561-756, South Korea

Electrospinning is the widely accepted technique for the fabrication of nanofibers from polymer solutions or melts using an electrostatic field. The nanofibers obtained by this technique possess unique characteristics like, high surface area, porous structure, flexibility, and component controllability. Because of these characteristics, electrospun nanofibers are being used extensively in biomedical applications, protective cloths, medicines, filtration, and composite reinforcement. Nanofibers with diameter ranging from50 to 100 nm or greater can be produced from this process; however, the properties of nanofibers depend on various parameters including properties of solution (viscosity, surface tension, and conductivity), applied electric potential, distance between needle tip to collector and atmospheric conditions (temperature, pressure and humidity) [29–31]. Also, electrospinning has been proven as a promising technique to obtain uniform dispersion of nanoparticles inside the nanofibers [32–34]. Till date, different types of nanofibers have been fabricated using this technique, such as nanofibers of organic polymer materials including synthetic and natural polymers and polymer nanofibers loaded with chromophores, nanoparticles, or active agents. On the other hand, metal and ceramics nanofibers cannot be electrospun directly although it is possible to fabricate either from their melts at extremely high temperature or by calcination/chemical conversion of precursor nanofibers containing polymer and inorganic precursor [29].

Therefore, present study aims to fabricate in situ-synthesized ZnS nanoparticles doped poly(vinyl)acetate nanofibers via cost-effective and versatile electrospinning technique. Interestingly, ZnS nanoparticles synthesized by adding ammonium sulfide solution to poly(vinyl acetate)/ZnAc sol-gel were incorporated inside polymer electrospun nanofibers. Thus obtained composite nanofibers are characterized using FE-SEM along with EDX, XRD, TEM, and FT-IR. Also, the nanofibers were investigated for antibacterial activity under indoor light activation toward Gram-negative and Gram-positive bacteria.

2 Experimental

2.1 Materials

Chemicals used in this work are zinc acetate dehydrate (ZnAc, Showa Chemical Ltd., Japan), N,N-dimethylformamide (DMF, Showa Chemical Ltd., Japan), poly(vinyl acetate) (PVAc, MW 5500,000 g/mol, Sigma-Aldrich), and ammonium sulfide ($(NH_4)_2S$, 40–48 wt% solution in water, Sigma-Aldrich). All the chemicals were used as received without further purification.

2.2 Fabrication of ZnS doped PVAc (ZnS-PVAc) elctrospun nanofibers

ZnS/PVAc colloidal solution was prepared in two steps. First, ZnAc/PVAc solution was prepared by adding ZnAc solution (ZnAc, 0.5 g in DMF, 2 ml) to 5 ml of 18 wt% PVAc/DMF solution under constant magnetic stirring. The resulting solution was continuously stirred for 2 h to ensure homogeneity. Secondly, 0.5 ml of ammonium sulfide was added carefully to ZnAc/PVAc solution dropwise under vigorous stirring. The final solution of ZnS/PVAc was kept under vigorous stirring for another 5 h to ensure fine dispersion of ZnS nanoparticles and electrospun by setting 15 kV applied voltage (high voltage power supply, CPS-60 K02 V1, Chungpa EMT, South Korea) and 15 cm tip to collector distance. The developing ZnS-PVAc electrospun nanofibers were collected on a drum collector rotating at constant speed. For the comparison of antibacterial activity, pristine PVAc nanofibers were also fabricated by the same process without ZnS nanoparticles. Electrospinning was carried out under atmospheric pressure, where temperature and relative humidity were maintained at about 25 °C and 60%, respectively. Afterwards, the nanofiber mats were vacuum-dried for 24 h to remove the residual solvent and used for further analysis. The schematic illustration for the fabrication of ZnS-PVAc electrospun nanofibers is shown in Fig. 1.

2.3 Characterization

Field emission scanning electron microscope (FE-SEM, S-7400, Hitachi, Japan) equipped with energy dispersive X-ray spectroscopy (EDS) was used to study the surface morphology of the nanofibers. Before characterization, samples were prepared by coating with platinum for 180 s using a Pt coater (E-1030, Hitachi). In the meantime, FE-SEM EDS spectrum of the nanofiber mats was also recorded. Information about the phase and crystallinity was obtained with a Rigaku X-ray diffractometer (XRD, Rigaku, Japan) with Cu Kα (λ = 1.540 Å) radiation over Bragg angles ranging from 10^o to 80^o. The distribution and high-resolution image of ZnS nanoparticles inside the polymer nanofibers were observed via transmission electron microscopy (TEM, JEM-2010, JEOL, Japan) with a 200 kV accelerating voltage. The samples were prepared by directly collecting the nanofibers on the TEM grid during electrospinning. The bonding configuration of the polymer with ZnS NPs was characterized using Fourier-transform infrared (FT-IR, FT/IR-4200, Jasco international Co., Ltd.).

2.4 Evaluation of antibacterial activity

The antibacterial susceptibility of two ATCC strains towards the ZnS-PVAc and pristine PVAc nanofibers was assessed using the disc diffusion method under indoor light conditions.

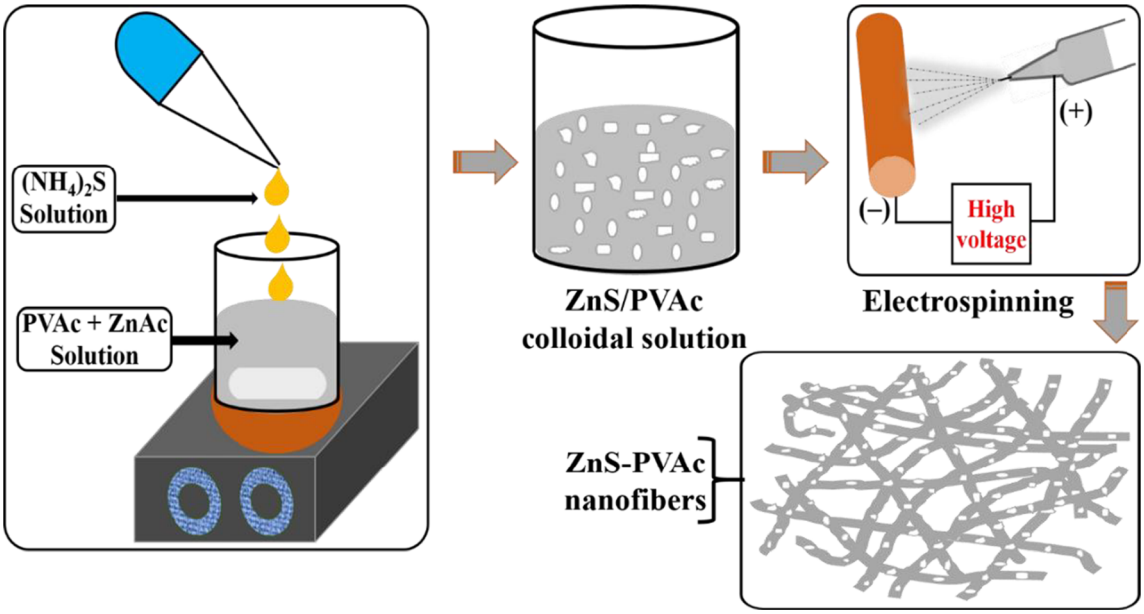

Fig. 1 Schematic illustration for the fabrication of ZnS-PVAc electrospun nanofibers

For this investigation, both the nanofiber mats were cut into circular disc of diameter around 5 mm each. The bacteria, *Escherichia coli (E. coli)* ATCC 25922 and *Staphylococcus aureus (S. aureus)* ATCC 25923 used in this study were obtained from Sukraraj Tropical and Infectious Disease Hospital, Teku, Kathmandu. Broth culture of *E. coli* and *S. aureus* were prepared on nutrient broth with OD_{600} measured between 0.08 and 0.12. The lawn culture of the organism was prepared by swabbing bacterial broth on the sterile, surface-dried MHA (Muller Hinton Agar) plate. Then the plate was left until the broth was completely soaked by the media. ZnS-PVAc nanofiber disc and pristine PVAc nanofiber disc (as control) were placed aseptically over the dried agar surface and incubated for 16–24 h at 37 °C. Finally, the growth of bacteria was observed, and the diameters of inhibition zones were measured.

3 Results and discussion

The surface morphology along with elemental composition of pristine PVAc and ZnS-PVAc electrospun nanofibers was characterized by FE-SEM/EDS (Fig. 2). Compared to pristine PVAc nanofibers, no any morphological difference was observed in ZnS-PVAc nanofibers (Fig. 2a & b). As shown in FE-SEM images, both pristine and doped nanofibers were found smooth, bead free, continuous and randomly oriented with uniform diameter ranging from 200 to 300 nm. Additionally, FE-SEM image of ZnS-PVAc nanofibers (Fig. 2b) confirmed the complete absence of nanoparticles on the surface of nanofibers indicating all the nanoparticles were incorporated inside the nanofibers. Moreover, the EDS analysis of ZnS-PVAc electrospun nanofibers revealed the presence of considerable amount of Zn and S (Fig. 2c). The spatial distribution of elements was represented by elemental mapping of ZnS-PVAc electrospun nanofibers (Fig. 3). As depicted in the figure, higher densities of C, Zn, and S are incorporated in the polymer chain suggesting good distribution of ZnS nanoparticles inside PVAc nanofibers.

In order to study the crystalline phase of fabricated samples, XRD analysis was performed (Fig. 4). The XRD patterns of pristine PVAc and ZnS-PVAc electrospun nanofiber mats displayed broad peaks at 2θ of 20° associated with the low crystallinity of PVAc. Conversely, the diffraction patterns of ZnS-PVAc nanofiber mat displayed three peaks at 2θ of 28.9°, 48.0°, and 58.0° corresponding to the crystallographic planes of (111), (220) and (311) in the cubic crystalline structure of ZnS (JCPDS, 77–2100). No peaks belonging to any other phase were detected.

The detailed study related to structure, morphological characteristics, and distribution of nanoparticles was provided by TEM and HR-TEM imaging (Fig. 5). Compared to the pristine PVAc nanofiber (Fig. 5a), ZnS-PVAc nanofiber contains uniformly distributed rice grain-shaped ZnS nanoparticles in it (Fig. 5b). The perfectly doped nanoparticles and the polymer fiber boundary were clearly visible in the HR-TEM image as shown in Fig. 5c. The particle diameter appeared to be around 5–10 nm in range. In addition, the HR-TEM image (Fig. 5c) expresses the good crystalline nature of ZnS nanoparticles; the lattice fringes with planar spacing of 0.32 nm represent the interplanar distance related to ZnS (111) plane, which is in good agreements with the standard value of the JCPDS, 77–2100. Here, we believe that this type of immobilization is due to the smaller size of nanoparticles than that of polymer

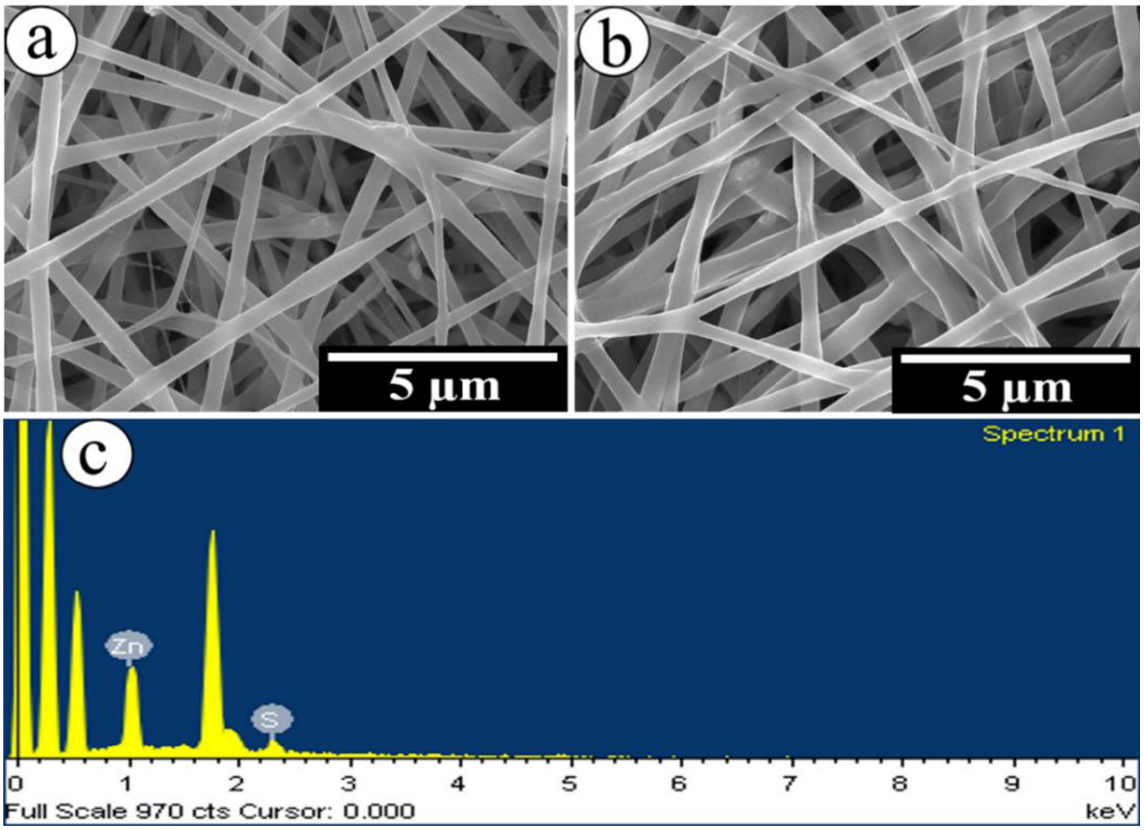

Fig. 2 FE-SEM images; **a** pristine PVAc electrospun nanofibers, **b** ZnS- PVAc electrospun nanofibers, and **c** EDS image of Fig. b

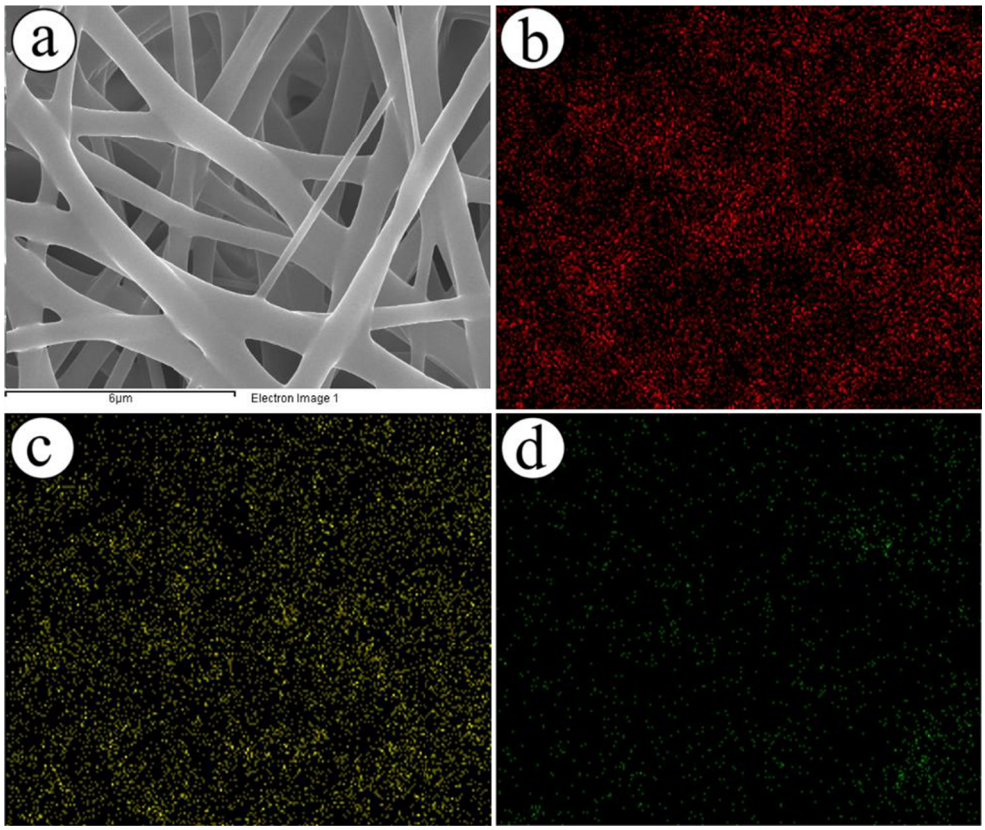

Fig. 3 Elemental mapping of ZnS- PVAc electrospun nanofibers; **a** FE-SEM image showing selected area for elemental mapping, **b** carbon, **c**, zinc, and **d** sulfur

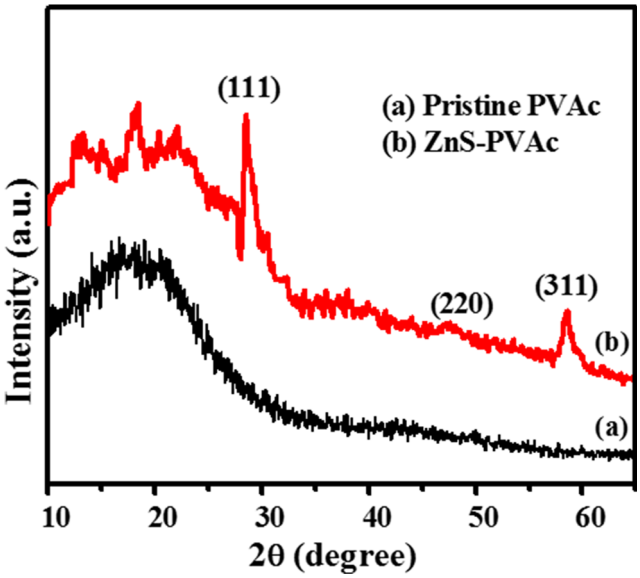

Fig. 4 XRD patterns; **a** pristine PVAc and **b** ZnS-PVAc electrospun nanofiber mats

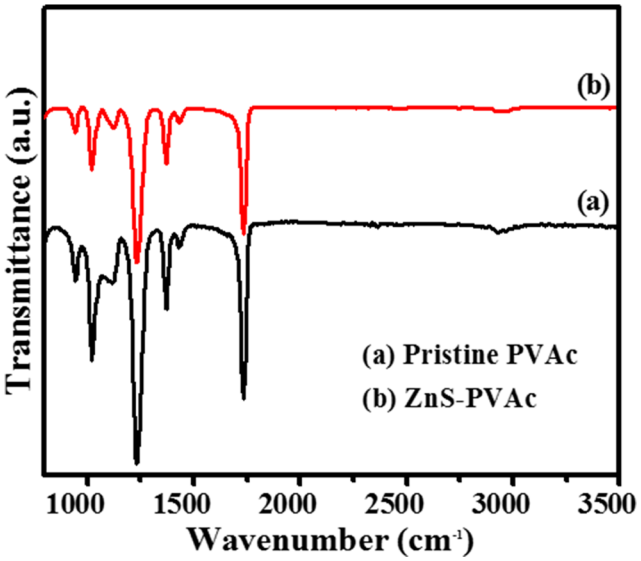

Fig. 6 FT-IR spectra; **a** pristine PVAc and **b** ZnS- PVAc electrospun nanofibers

nanofibers [28]. The homogenous distribution of ZnS nanoparticles inside the polymer nanofibers might be assigned to the coulombic repulsion between charged metallic nanoparticles (M^{2+}) during electrospinning.

The influence on the structure of PVAc due to incorporation of ZnS nanoparticles was investigated using FT-IR spectroscopy. Figure 6 shows the FT-IR spectra of pristine PVAc and ZnS-PVAc electrospun nanofibers. The peak at 1739.4 cm^{-1} ($\nu_{c=o}$) and characteristic peaks at 1239.9, 1020.9 cm^{-1} ($\nu_{c\text{-}o}$), and 1375.7 cm^{-1} (δCH_3) corresponding to PVAc are clearly seen. The FT-IR spectrum is similar to the standard IR spectrum curve of PVAc (Sprouse collection of IR, card no. 187–189) [35]. The ZnS-PVAc nanofibers also showed the similar patterns to that of pure PVAc nanofibers with some reduced intensity. This may have occurred due to the presence of ZnS nanoparticles in the PVAc. Therefore, FT-IR spectrum indicates and confirms that PVAc was not affected by the synthesizing procedure of ZnS. Furthermore, these results indicated that the proposed fabrication strategy could embed ZnS nanoparticles inside the PVAc nanofiber without influencing its structural changes.

The bactericidal effect of ZnS is already well-known and has been studied for many years [36, 37]. Antibacterial activity of the ZnS-PVAc nanofibers is shown in Fig. 7. It is well-known that when an antibacterial material is in contact with bacterial strain, a clear area (zone of inhibition) around the antibacterial material is formed [38]. The strain susceptible to antibacterial agent exhibits a larger diameter, while resistant strain exhibits smaller diameter of inhibition zone. As shown in the Figure, pristine PVAc samples showed no zones of inhibition, suggesting the absence of antibacterial activity for both bacterial strains, mainly due to lack of ZnS nanoparticles. On the other hand, ZnS-PVAc nanofibers clearly showed distinct area of zone of inhibition for both bacterial strains. In spite of low content and indoor light activation of ZnS nanoparticles confined in polymer nanofibers, the results obtained

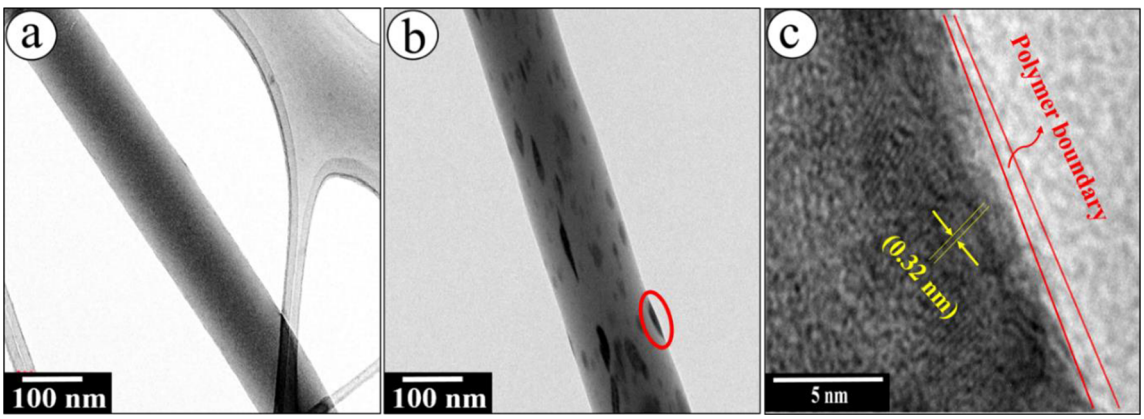

Fig. 5 TEM images; **a** pristine PVAc and **b** ZnS-PVAc electrospun nanofiber. Panel **c** represents the HR-TEM image of marked area of **b**

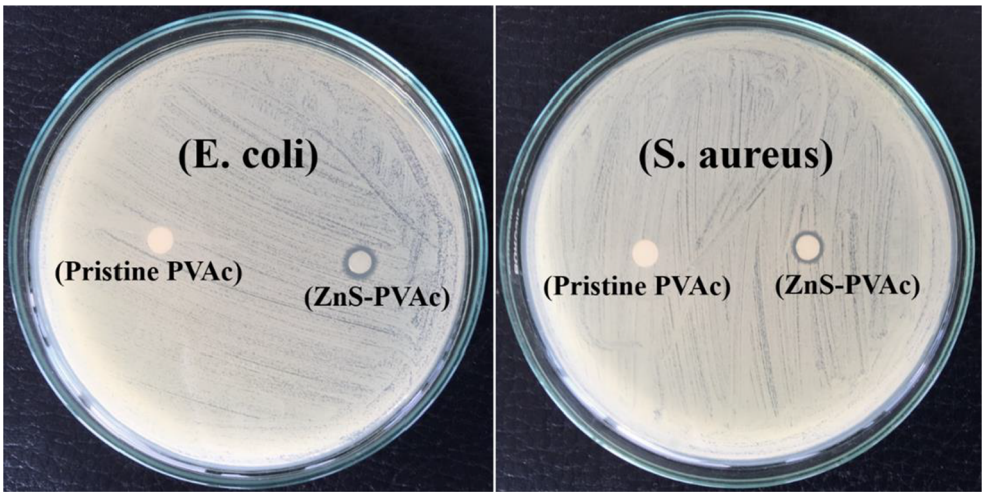

Fig. 7 Bactericidal activity; pristine PVAc and ZnS-PVAc electrospun nanofiber mat with *E. coli* and *S. aureus* bacteria

were promising. The zone of inhibition were 9 mm and 8 mm for *E. coli* and *S. aureus*, respectively. The higher zone of inhibition for *E. coli* compared to that of *S. aureus* might be related to the cellular wall thickness and content differences between Gram-negative and Gram-positive bacteria. Gram-positive bacteria possess continuous thick cell wall (20–80 nm) consisting mainly of peptidoglycane, whereas Gram-negative bacteria possess thinner layer of peptidoglycane (5–10 nm) surrounded by an outer phospholipidic membrane [39]. Finally, bactericidal activity of ZnS along with PVAc nanofibers may offer great promise to its application in pharmaceutical industries.

The possible mechanism for the antibacterial action of ZnS-PVAc nanofibers can be explained on the basis of published report [40]. ZnS being a semiconductor material can generate biologically reactive oxygen species (ROS) inducing hydroxyl radical ($OH^{\bullet}$) under UV-light irradiation due to its high band gap. However, this work attempts the indoor light activation of ZnS to produce ROS. During activation process, holes (h^{+}) and electrons (e) are generated in valence band (VB) and conduction band (CB), respectively. Low recombination of photogenerated holes and electrons is an important characteristic. So it can be occurred significantly with the decrease in particle size of semiconductor to nanoscale level.

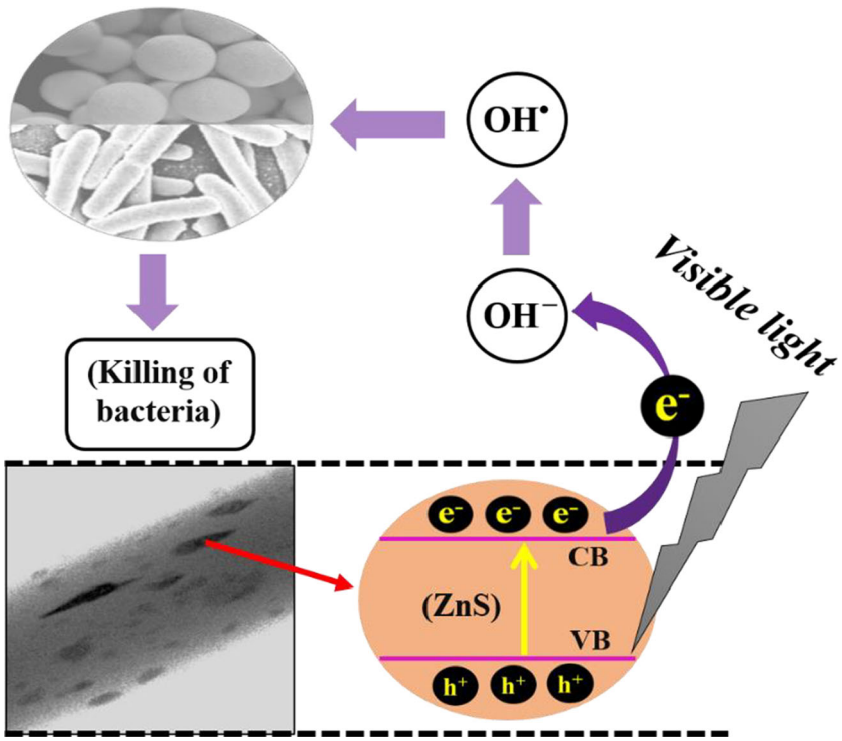

Fig. 8 Schematic illustration showing the degradation of cell membrane of bacteria by biologically reactive oxygen species

During indoor light activation, holes at VB get trapped by hydroxyl groups (OH^-) or water (H_2O) on ZnS surface to produce hydroxide radicals ($OH^•$). Meanwhile, the good conductivity of PVAc polymer (due to the presence of active CH_3 groups) plays an important role to transfer excited electrons from CB of ZnS to the surface of nanofibers, where they react with dissolved oxygen molecules to yield superoxide radical ions ($O_2^{•-}$) [41]. The $O_2^{•-}$, after protonation generate hydroperoxide radicals ($HO_2^•$) leading to the formation of $OH^•$. Thus, produced $OH^•$ are responsible to assist the degradation of cell membrane of bacteria leading to the loss of cellular components and cell death [42, 43]. The conceptual mechanism for degradation of bacterial cell membrane is illustrated in Fig. 8. The reactions, which take place during the formation of ROS are summarized as follows [44]:

$$ZnS + hv \rightarrow h^+(VB) + e^-(CB)$$

At valence band:

$$h^+ + H_2O \rightarrow OH^+ + OH^•$$
$$h^+ + OH^- \rightarrow OH^•$$

At conduction band:

$$e^- + O_2 \rightarrow O_2^{•-}$$
$$O_2^{•-} + H^+ \rightarrow HO_2^•$$
$$2HO_2^• \rightarrow H_2O_2 + O_2$$
$$H_2O_2 + O_2^{•-} \rightarrow OH^- + OH^• + O_2$$
$$H_2O_2 + e^- \rightarrow OH^- + OH^•$$
$$OH^• + \text{Bacteria} \rightarrow \text{degradation of cell membrane}$$

4 Conclusion

Rice grain-shaped ZnS nanoparticles doped PVAc (ZnS-PVAc) nanofibers were fabricated by electrospinning of ZnS/PVAc colloid. FE-SEM and TEM analysis revealed that the ZnS nanoparticles were completely embedded inside the polymer nanofibers. The formed ZnS-PVAc nanofibers exhibited promising antibacterial activity over *E. coli* and *S. aureus* under indoor light activation. Experimental results showed that encapsulation of ZnS nanoparticles did not affect the antibacterial activity of ZnS-PVAc nanofibers. Moreover, the introduced strategy could overcome the photocorrosion and recovery problems of nanoparticles after their use. Overall, this work can provide a new path to design low-cost, reusable, and healthily safe Zn-based nanoparticles doped polymer nanofibers via electrospinning.

Funding information This research was supported by Traditional Culture Convergence Research Program through the National Research Foundation of Korea (NRF) funded by the Ministry of Science, CT & Future Planning (2018M3C1B5052283) and National Research Foundation of Korea (NRF) grant funded by the Korea Government (MSIT) (No.NRF-2019R1A2C1004467).

Compliance with ethical standards

Conflict of interest The authors declare that they have no conflict of interest.

References

1. Roduner E (2006) Size matters: why nanomaterials are different. Chem Soc Rev 35:583–592
2. Wang Y, Herron N (1991) Nanometer-sized semiconductor clusters: materials synthesis, quantum size effects, and photophysical properties. J Phys Chem 95:525–532
3. Yan L, Li Q, Chi H, Qiao Y, Zhang T, Zheng F (2018) One-pot synthesis of acrylate resin and ZnO nanowires composite for enhancing oil absorption capacity and oil-water separation. Adv Compos Hybrid Mater 1:567–576
4. Zhao X, Li H, Wang HS, Zhong Z (2011) Preparation of mesoporous Ag-TiO_2 thin films by a simple photocatalytic deposition method and their application as photocatalyst. Sci Adv Mater 3: 984–988
5. Xiao X, Zhang WD (2011) One-step hydrothermal synthesis, characterization and photocatalytic properties of nano TiO_2 with controllable crystalline structure. J Nanoeng Nanomanuf 1:287–291
6. Thomas J, Kumar KP, Mathew S (2011) Enhancement of sunlight photocatalysis of nano TiO_2 by Ag nanoparticles stabilized with d-glucosamine. Sci Adv Mater 3:59–65
7. Michalet X, Pinaud FF, Bentolila LA, Tsay JM, Doose S, Li JJ, Sundaresan G, Wu AM, Gambhir SS, Weiss S (2005) Quantum dots for live cells, in vivo imaging, and diagnostics. Science 307: 538–544
8. Dutta RK, Sharma PK, Bhargava R, Kumar N, Pandey AC (2010) Differential susceptibility of Escherichia coli cells toward transition metal-doped and matrixembedded ZnO nanoparticles. J Phys Chem B 114:5594
9. Yun YH, Youn HG, Shin JY, Yoon SD (2017) Preparation of functional chitosan-based nanocomposite film containing ZnS nanoparticles. Int J Biol Macromol 104:1150–1157
10. Ding JX, Zapien JA, Chen WW, Lifshitz Y, Lee ST, Meng XM (2004) Lasing in ZnS nanowires grown on anodic aluminum oxide templates. Appl Phys Lett 85:2361
11. Fang X, Bando Y, Liao M, Gautam UK, Zhi C, Dierre B, Liu B, Zhai T, Sekiguchi T, Koide Y, Golberg D (2009) Single-crystalline ZnS Nanobelts as ultraviolet-light sensors. Adv Mater 21:2034–2039
12. Yu SH, Yoshimura M (2002) Shape and Phase Control of ZnS Nanocrystals: Template Fabrication of Wurtzite ZnS Single-Crystal Nanosheets and ZnO Flake-like Dendrites from a Lamellar Molecular Precursor $ZnS{\cdot}(NH_2CH_2CH_2NH_2)_{0.5}$. Adv Mater 14:296–300
13. Wada Y, Yin H, Yanagida S (2002) Environmental remediation using catalysis driven under electromagnetic irradiation. Catal Surv Jpn 5:127–138
14. Fang X, Bando Y, Shen G, Ye C, Gautam UK, Pedro M, Costa FJ, Zhi C, Tang C, Golberg D (2007) Ultrafine ZnS Nanobelts as Field Emitters. Adv Mater 19:2593–2596
15. Feigl C, Russo SP, Barbard AS (2010) Safe, stable and effective nanotechnology: phase mapping of ZnS nanoparticles. J Mater Chem 20:4971–4980

16. Bang JH, Helmich RJ, Suslich KS (2008) Nanostructured ZnS:Ni^{2+} Photocatalysts prepared by ultrasonic spray pyrolysis. Adv Mater 20:2599–2603
17. Barrocas B, Entradas TJ, Nunes CD, Monteiro OC (2017) Titanate nanofibers sensitized with ZnS and Ag_2S nanoparticles as novel photocatalysts for phenol removal. Appl Catal B Environ 218: 709–720
18. Zhang X, Liu X, Zhang L, Li D, Liu S (2016) Novel porous Ag_2S/ZnS composite nanosphere: fabrication and enhanced visible light photocatalytic activities. J Alloys Compd 655:38–43
19. Mizuhata M, Mineyama Y, Maki H (2016) Fabrication of ZnS/porous silicon composite and its enhancement of photoluminescence. Electrochim Acta 201:86–95
20. Xie Y, Zhang C, Miao S, Liu Z, Ding K, Miao Z, An G, Yang Z (2008) One-pot synthesis of ZnS/polymer composites in supercritical CO_2-ethanol solution and their applications in degradation of dyes. J Colloid and Interface Sci 318:310–315
21. Bai J, Li Y, Jin P, Wang J, Liu L (2017) Facile preparation 3D ZnS nanospheres-reduced graphene oxide composites for enhanced photodegradation of norfloxacin. J Alloys Compd 729:809–815
22. Tang Y, Tian J, Malkoske T, Li W, Chen B (2017) Facile ultrasonic synthesis of novel zinc sulfide/carbon nanotube coaxial nanocables for enhanced photodegradation of methyl orange. J Mater Sci 52: 1581–1589
23. Chang CJ, Chu KW, Hsu MH, Chen CY (2015) Ni-doped ZnS decorated graphene composites with enhanced photocatalytic hydrogen-production performance. Int J Hydrog Energy 40: 14498–14506
24. Farhadi S, Siadatnasab F, Khataee A (2017) Ultrasound-assisted degradation of organic dyes over magnetic $CoFe_2O_4$@ZnS core-shell nanocomposite. Ultrason Sonochem 37:298–309
25. Xie Y, Qiao ZP, Chen M, Liu XM, Qian YT (1999) Irradiation route to semiconductor/polymer nanocable fabrication. Adv Mater 11: 1512–1515
26. Choi IS, Li XH, Simanek EE, Akaba R, Whitesides GM (1999) Self-assembly of hydrogen-bonded polymeric rods based on the cyanuric acid·melamine lattice. Chem Mater 11:684–690
27. Panthi G, Park SJ, Kim TW, Chung HJ, Hong ST, Park M, Kim HY (2015) Electrospun composite nanofibers of polyacrylonitrile and Ag_2CO_3 nanoparticles for visible light photocatalysis and antibacterial applications. J Mater Sci 50:4477–4485
28. Barakat NAM, Abadirc MF, Sheikh FA, Kanjwal MA, Park SJ, Kim HY (2010) Polymeric nanofibers containing solid nanoparticles prepared by electrospinning and their applications. Chem Eng J 156:487–495
29. Panthi G, Park M, Kim HY, Lee SY, Park SJ (2015) Electrospun ZnO hybrid nanofibers for photodegradation of wastewater containing organic dyes: a review. J Ind Eng Chem 21:26–35
30. Yang S, Liu Y, Jiang Z, Gu J, Zhang D (2018) Thermal and mechanical performance of electrospun chitosan/poly(vinyl alcohol) nanofibers with graphene oxide. Adv Compos Hybrid Mater 1: 722–730
31. Görgün N, Özer C, Polat K (2019) A new catalyst material from electrospun PVDF-HFP nanofibers by using magnetron-sputter coating for the treatment of dye-polluted waters. Adv Compos Hybrid Mater 2:423–430
32. Gu J, Lv Z, Wu Y, Guo Y, Tian L, Qui H, Li W, Zhang Q (2017) Dielectric thermally conductive boron nitride/polyamide composites with outstanding thermal stabilities via in-situ polymerization electrospinning-hot press method. Compos Part A 94:209–216
33. Ruan K, Guo Y, Tang Y, Zhang Y, Zhang J, He M, Kong J, Gu J (2018) Improved thermal conductivities in polystyrene nanocomposites by incorporating thermal reduced graphene oxide via electrospinning-hot press technique. Compos Commun 10:68–72
34. Guo Y, Lyu Z, Yang X, Lu Y, Ruan K, Wu Y, Kong J, Gu J (2019) Enhanced thermal conductivities and decreased thermal resistances of functionalized boron nitride/polyamide composites. Composites Part B 164:732–739
35. Panthi G, Barakat NAM, Park M, Kim HY, Park SJ (2015) Fabrication of PdS/ZnS NPs doped PVAc hybrid electrospun nanofibers: effective and reusable catalyst for dye photodegradation. J Ind Eng Chem 21:298–302
36. Synnott DW, Seery MK, Hinder SJ, Michlits G, Pillai SC (2013) Antibacterial activity of indoor-light activated photocatalysts. Appl Catal B Environ 130-131:106–111
37. Kumar GA, Naik HSB, Viswanath R, Gowda IKS, Santhosh KN (2017) Tunable emission property of biotin capped Gd:ZnS nanoparticles and their antibacterial activity. Mater Sci Semicond Process 58:22–29
38. Gallent-Behm CL, Yin HQ, Liu SJ, Hegger JP, Langford RE, Olson ME, Hart DA, Burrel RE (2005) Comparison of in vitro disc diffusion and time kill-kinetic assays for the evaluation of antimicrobial wound dressing efficacy. Wound Repair Regen 13:412–421
39. Amato E, Diaz-Fernandez YA, Taglietti A, Pallavicini P, Pasotti L, Cucca L, Milanese C, Grisoli P, Dacarro C, Fernandez-Hechayarria JM, Necchi V (2011) Synthesis, characterization and antibacterial activity against gram positive and gram negative Bacteria of biomimetically coated silver nanoparticles. Langmuir 27:9165–9173
40. He W, Jia H, Cai J, Han X, Zheng Z, Wamer WG, Yin J (2016) Production of reactive oxygen species and electrons from photoexcited ZnO and ZnS nanoparticles: a comparative study for unraveling their distinct photocatalytic activities. J Phys Chem C 120:3187–3195
41. Afeesh R, Barakat NAM, Al-Deyab SS, Yousef A, Kim HK (2012) Nematic shaped cadmium sulfide doped electrospun nanofiber mat: highly efficient, reusable, solar light photocatalyst. Collid Surface A 409:21–29
42. Kiwi J, Nadtochenko V (2005) Evidence for the mechanism of photocatalytic degradation of the bacterial wall membrane at the TiO_2 interface by ATR-FTIR and laser kinetic spectroscopy. Langmuir 21:4631–4641
43. Li Y, Zhang W, Niu J, Chen Y (2012) Mechanism of Photogenerated reactive oxygen species and correlation with the antibacterial properties of engineered metal-oxide nanoparticles. ACS Nano 6:5164–5173
44. Kaur S, Sharma S, Umar A, Singh S, Mehta SK, Kansal SK (2017) Solar light driven enhanced photocatalytic degradation of brilliant green dye based on ZnS quantum dots. Superlattice Microst 103: 365–375